

DELAYED IMPLANTATION OF INTRAMEDULLARY CHITOSAN CHANNELS CONTAINING NERVE GRAFTS PROMOTES EXTENSIVE AXONAL REGENERATION AFTER SPINAL CORD INJURY

Hiroshi Nomura, M.D., Ph.D.

Toronto Western Research Institute,
Toronto Western Hospital,
Toronto, Canada

Bilal Baladie, Ph.D.

Department of Chemical Engineering
and Applied Chemistry,
University of Toronto, and
Department of Chemistry,
Institute of Biomaterials and
Biomedical Engineering,
Toronto, Canada

Yusuke Katayama, M.A.Sc.

matREGEN,
Toronto, Canada

Cindi M. Morshead, Ph.D.

Department of Surgery and
Institute of Medical Sciences,
University of Toronto, and
Terrence Donnelly Centre for Cellular
and Biomolecular Research,
Toronto, Canada

Molly S. Shoichet, Ph.D.

Department of Chemical Engineering
and Applied Chemistry,
University of Toronto, and
Department of Chemistry,
Institute of Biomaterials and
Biomedical Engineering,
Terrence Donnelly Centre for Cellular
and Biomolecular Research,
Toronto, Canada

Charles H. Tator, M.D., Ph.D.

Toronto Western Research Institute,
Toronto Western Hospital and
University of Toronto,
Toronto, Canada

Reprint requests:

Charles H. Tator, M.D., Ph.D.,
Toronto Western Research Institute,
Toronto Western Hospital and
University of Toronto,
Room 12-435, McLaughlin Wing,
399 Bathurst Street,
Toronto, Ontario, Canada M5T 2S8.
Email: charles.tator@uhn.on.ca

Received, October 19, 2007.

Accepted, March 10, 2008.

OBJECTIVE: We describe a new strategy to promote axonal regeneration after subacute or chronic spinal cord injury consisting of intramedullary implantation of chitosan guidance channels containing peripheral nerve (PN) grafts.

METHODS: Chitosan channels filled with PN grafts harvested from green fluorescent protein rats were implanted in the cavity 1 week (subacute) or 4 weeks (chronic) after 50-g clip injury at T8 and were compared with similarly injured animals implanted with either unfilled channels or no channels. Functional recovery was measured weekly for 12 weeks by open-field locomotion, after which histological examination was performed.

RESULTS: The implanted channels with PN grafts contained a thick tissue bridge containing as many as 35,000 myelinated axons in both the subacute and chronic spinal cord injury groups, with the greatest number of axons in the channels containing PN grafts implanted subacutely. There were numerous green fluorescent protein-positive donor Schwann cells in the tissue bridges in all animals with PN grafts. Moreover, these Schwann cells had high functional capacity in terms of myelination of the axons in the channels. In addition, PN-filled chitosan channels showed excellent biocompatibility with the adjacent neural tissue and no obvious signs of degradation and minimal tissue reaction at 14 weeks after implantation. In control animals that had unfilled chitosan channels implanted, there was minimal axonal regeneration in the channels; in control animals without channels, there were large cavities in the spinal cords, and the bridges contained only a small number of axons and Schwann cells. Despite the large numbers of axons in the chitosan channel–PN graft group, there was no significant difference in functional recovery between treatment and control groups.

CONCLUSION: Intramedullary implantation of chitosan guidance channels containing PN grafts in the cavity after subacute spinal cord injury resulted in a thicker bridge containing a larger number of myelinated axons compared with chitosan channels alone. A chitosan channel containing PN grafts is a promising strategy for spinal cord repair.

KEY WORDS: Axonal regeneration, Channel implantation, Chitosan, Peripheral nerve grafts, Spinal cord clip compression injury, Spinal cord injury

Neurosurgery 63:127–143, 2008

DOI: 10.1227/01.NEU.0000316443.88403.16

www.neurosurgery-online.com

In recent years, tissue engineering has been applied to the field of spinal cord injury (SCI) repair (16, 31). One of the most promising strategies is to bridge the cavity created by SCI with synthetic scaffolds that promote axonal regrowth and provide a protected environment hospitable to regeneration (see Nomura et al. [31] for a thorough review of the synthetic biomaterials used to stimulate axonal

regeneration in experimental SCI). For repair of SCI, three types of synthetic scaffolds, gels, sponges, and tubes, have been used to reconstruct the damaged spinal cord. On the one hand, gels and sponges are advantageous for filling the posttraumatic cavity and as vehicles to uniformly disperse cells or drugs, although they do not provide a straight pathway to guide regenerating axons through the lesion.

For example, plain collagen filaments enhanced functional recovery after complete spinal cord transection (SCT) (57), and a methacrylamide hydrogel inserted into the cavity in a chronic SCI model produced some axonal regrowth and proliferation of blood vessels (55). On the other hand, tubular channels provide a straight pathway for regenerating axons to bridge the lesion. Our group previously showed that empty methacrylate-based hydrogel channels allowed ingrowth of a small number of regenerating axons after SCT, showing that a synthetic conduit itself could stimulate axonal regrowth (48). For human application, degradable channels are favored to avoid permanent implantation or a second operation for their removal (17). However, biodegradable channels have a propensity to collapse owing to insufficient wall strength (18). The ideal scaffold would slowly degrade over several months to allow sufficient time for axonal regeneration.

For repair of SCI, tubular synthetic channels have been combined with transplanted cells, such as Schwann cells (10) and olfactory ensheathing glia (36), and have shown potential to induce axonal sprouting from the injured spinal cord. Biocompatibility of the biomaterials is essential for this combination strategy of channels and cell transplants. Also, absorbable channels must remain intact and patent for sufficiently long periods of time to allow axonal regeneration, and although there are some successful materials that meet these criteria, it is difficult to control the degradation rate precisely (32). Our group is interested in examining biomaterials with slow degradation and good biocompatibility for combination strategies for subacute and chronic spinal cord repair. Although some combinatorial strategies of tubular channels containing transplanted cells have been performed in acute models of complete or incomplete SCT (11, 21, 56), we are not aware of any reports of synthetic channel implantation in chronic SCI.

Chitosan is a naturally occurring polysaccharide derived from the exoskeletons of crustaceans and insects (16, 30). Because it is nontoxic, biocompatible, and biodegradable, chitosan channels have been used as artificial bridges for repair in sciatic nerve injury in rodents (22) and dogs (43). Furthermore, a chitosan tubular scaffold containing cultured Schwann cells has been used in peripheral nerve (PN) repair in rodents (59).

In the present study, we examined delayed intracavitary implantation of chitosan channels after 1 week (subacute) or 4 weeks (chronic) in a model of severe compression SCI. We compared an injured group transplanted with chitosan channels filled with PN grafts to injured groups with either empty chitosan channels or no channels, and assessed axonal regeneration and functional recovery. To distinguish donor Schwann cells from host Schwann cells in the channel, the PN grafts were harvested from green fluorescent protein (GFP) rats and implanted in non-GFP rats. Three features of the present study are unique for spinal cord repair: 1) intracavitary implantation of a guidance channel in a nontransection model of subacute and chronic SCI; 2) implantation of a guidance channel composed of chitosan; and 3) use of GFP PN allografts.

MATERIALS AND METHODS

Production of Channels

Five grams of medical-grade chitosan (Protosan UP CL 213; NovaMatrix, Drammen, Norway) was dissolved in 500 ml of distilled water, and the chitosan solution was precipitated using 40 ml of 4% wt/wt of NaOH. Precipitated chitosan flakes were filtered and rinsed several times with distilled water until neutralization. After freeze drying, the chitosan solution was prepared by dissolving 3% wt/wt chitosan in 2% vol/vol acetic acid. Then, 2.5 ml of the solution was mixed vigorously with 2.5 ml of ethanol and stored at 4°C. Ninety-one μ l of acetic anhydride was added to the previous chitosan solution (5 ml total) and the mixture was stirred, degassed, and injected into a glass mold (diameter, 5 mm; length, 27 cm) cored with a stainless steel rod (diameter, 2 mm; length, 27 cm). After injection, the glass mold was allowed to set for 24 hours to allow the conversion of chitosan to a chitin hydrogel. The gelled chitin tube was removed from the core's mold and washed vigorously with distilled water to remove excess acetic acid by-product. The washed chitin channel was then removed from the 2-mm glass tubes, placed in 1.6-mm glass tubes, and deacetylated (to convert chitin to chitosan) using 40% wt/vol of NaOH. For deacetylation, the channels were heated at 110°C for three cycles, each for 2 hours, and washed with distilled water after each cycle of deacetylation into 92% deacetylation. The chitosan channels were then washed thoroughly with distilled water until a pH of 7 was obtained. They were then removed from the 1.6-mm mold and placed in a 1.45-mm mold for resizing. The channels were dried in air for approximately 1 hour, then wetted again before removal from the mold. The channels were cut into 8-mm lengths, dried, and sterilized by ethylene oxide gas. The channels were approximately 1.8 mm in outer diameter and the wall thickness was 0.2 mm (16). The channels were sterilized by ethylene oxide gas before implantation.

Animals

Sixty-four wild-type adult female Sprague Dawley (SD) rats (288 ± 21 g; Charles River, St. Constant, Canada) and 25 adult GFP transgenic Wistar rats (Wistar-TgN(CAG-GFP)184ys); bred in the laboratory of Dr. Armand Keating, (Toronto, Canada, 297 ± 61 g) were used in this study. The transgenic rats were originally obtained from the YS Institute, Inc., Utsunomiya, Tochigi, Japan. The animal protocols were approved by the Animal Care Committee of the Research Institute of the University Health Network in accordance with policies established by the Canadian Council on Animal Care. The SD rats were divided into subacute and chronic groups depending on the interval between the spinal cord compression injury and the second operation for channel implantation, 1 or 4 weeks later, respectively. For channel implantation, each of the subacute and chronic groups was divided into three subgroups. The designations used are defined as follows: subacute (SA), chronic (CH), channel with PN grafts (C+PN), empty channel (EC), and no channel (N). Subgroups 1, 2, and 3 in the subacute group are designated subacute channel + PN (Group SA+C+PN), subacute empty channel (Group SA+EC), and subacute no channel (Group SA+N), respectively. Subgroups 1, 2, and 3 in the chronic group are designated as chronic channel + PN (Group CH+C+PN), chronic empty channel (Group CH+EC), and chronic no channel (Group CH+N), respectively. The number of animals in each subgroup is shown in *Table 1*.

Spinal Cord Clip Compression Injury

Sixty-four SD rats were deeply anesthetized with 2% halothane with 1:2 nitrous oxide to oxygen and received 5 ml of saline subcutaneously. Laminectomy at the T7–T9 level was performed, then the spinal cord

TABLE 1. Number of animals for each analysis^a

Group	Total no.	Wall thickness	Paraffin	Frozen	BDA	TEM	Cavity length	Axon counts
Subacute								
1a	11	4	3	3	3	1	—	4
1b	10	4	3	2	2	1	—	4
1c	10	—	8	2	2	—	8	—
Total	31							
Chronic								
2a	12	4	5	2	2	1	—	4
2b	10	4	3	2	2	1	—	4
2c	11	—	9	2	2	—	9	—
Total	33							

^a BDA, biotin dextran amine; TEM, transmission electron microscopy. Subacute and chronic groups contain animals treated secondly in surgery 1 and 4 weeks after clip injury, respectively. Groups 1a and 2a, channel implantation containing peripheral nerve grafts 1 and 4 weeks after clip injury, respectively. Groups 1b and 2b, empty channel implantation 1 and 4 weeks after clip injury, respectively. Groups 1c and 2c, no channel implantation 1 and 4 weeks after clip injury, respectively.

was compressed at T8 by a 50-g clip for 1 minute (Fig. 1A), as originally described by Rivlin and Tator (42). After the clip was removed, the dorsal aspect of the compressed spinal cord was covered by a syn-

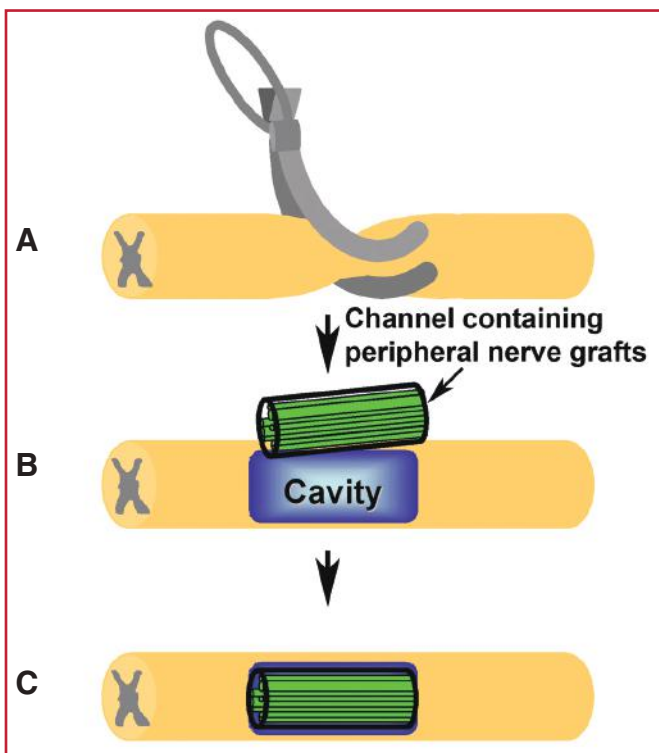


FIGURE 1. Diagrams showing the surgical procedures for implantation of chitosan channels containing peripheral nerve (PN) grafts. **A**, after laminectomy at T7–T9, the spinal cord was compressed at T8 with a 50-g clip for 1 minute. **B**, at 1 week or 4 weeks after clip injury, a dorsal myelotomy was created to enter the cavitated injury site for channel implantation. **C**, a channel containing PN grafts from a green fluorescent protein (GFP) rat was then implanted in the cavity.

thetic expanded polytetrafluoroethylene membrane (Preclude Gore-Tex Dura Substitute; Gore & Associates, Inc., Flagstaff, AZ) to prevent extradural scarring and invasion of fibrous tissue. The incision was closed with 3–0 Vicryl sutures (Johnson & Johnson, Peterborough, Canada) in the paravertebral muscles and Michel clips (Fine Science Tools, North Vancouver, Canada) in the skin.

All animals received buprenorphine (0.03 mg/kg) subcutaneously for 3 days postinjury and manual bladder compression three times daily. Urinary tract infections were treated with ampicillin (0.17 mg/g every 12 hr subcutaneously) for 5 days.

Functional recovery was analyzed at 1 week after SCI in the subacute groups or weekly for 4 weeks in the chronic groups using the Basso, Beattie, and Bresnahan (BBB) open-field locomotor test (6). BBB scoring was conducted by three observers blinded to the experimental group. Each animal was scored and videotaped for 4 minutes each week.

Harvesting of PN Grafts from GFP Rats

For harvesting GFP-positive PN grafts, 23 GFP Wistar rats were deeply anesthetized with 2% halothane and then 3:1 nitrous oxide to oxygen. Eleven rats were used for Group SA+C+PN and 12 for Group CH+C+PN. Ten intercostal nerves were harvested per animal from T7 to T11 bilaterally and preserved in Hanks' buffered saline solution. Each harvested nerve was approximately 15 mm in length. After harvesting, the GFP rats were sacrificed with an overdose of halothane. Sterilized dried chitosan channels approximately 7 mm in length were immersed in Hanks' buffered saline for at least 2 minutes until they softened and expanded to approximately 8 mm in length. The 10 nerves were stacked in a bundle, and one end of the bundle was encircled by an 8–0 Vicryl suture that was then tied snugly to hold the 10 nerves together. The suture was then inserted into the channel, and the bundle of nerves pulled into the channel. Nerves protruding beyond the channel were trimmed with microscissors, then the channels were placed in Hanks' buffered saline until implantation.

Intramedullary Implantation of the Chitosan Channels into the Cavity after SCI

Channel implantation was performed at a second operation 1 week after clip injury in the subacute groups ($n = 31$) or 4 weeks after injury in the chronic groups ($n = 33$). The SD rats were deeply anesthetized

with 2% halothane with 1:2 nitrous oxide to oxygen, the previous operative site was reopened, and after removing the Gore-Tex membrane on the dorsal surface of the injured spinal cord, the dura mater was incised longitudinally with microscissors from T7 to T9. There was focal atrophy of the cord and cavitation from the clip injury. A dorsal midline myelotomy of 5 mm in length was created longitudinally at the SCI site with a no. 11 surgical blade (Feather; Ohyodo-Minami, Osaka, Japan) and microscissors, avoiding the dorsal spinal vein. Trauma to the spared spinal cord tissue was minimized by dissection strictly in the midline through the dorsal medial septum to reach the cavity. A small piece of absorbable gelatin sponge (Surgifoam; Ethicon, Inc., Soeborg, Denmark) was inserted temporarily in the cavity to control any hemorrhage. Then, a channel containing PN grafts or an empty channel was implanted in the cavity (Fig. 1, B and C). In the empty channel groups, the chitosan channels were prepared identically to the filled channels, except that the PN grafts were omitted. After channel implantation, the dorsal aspect of the channel was covered with 40 μ l of fibrin sealant Beriplast P (gift from ZLB Behring GmbH, Marburg, Germany), and the Gore-Tex membrane was repositioned to cover the entire spinal cord including the site of channel implantation. A bilateral spinal fusion was then performed from T6 to T10 with no. 5 surgical steel (Ethicon, Inc., Somerville, NJ) and 2-0 silk (Johnson & Johnson) using a method that we reported previously (30). At the second operation, in Groups SA+N and CH+N (the no-channel subgroups), a spinal fusion from T6 to T10 was also performed, but without dorsal myelotomy or channel implantation. The incisions were closed with 3-0 Vicryl sutures in the paravertebral muscles and Michel clips in the skin.

All animals received buprenorphine (0.03 mg/kg) subcutaneously for 3 days and manual bladder compression three times daily until spontaneous voiding was reestablished. Because the SD rats in Groups SA+C+PN and CH+C+PN had PN grafts harvested from GFP Wistar rats, all animals received cyclosporine (10 mg/kg) for immunosuppression (Sandimmune; Nacartis Pharma Canada, Inc., Dorval, Canada) injected subcutaneously daily until they were sacrificed. Functional recovery was assessed weekly by BBB testing for an additional 12 weeks after the second operation using the same techniques.

Anterograde Axonal Tracing with Biotin Dextran Amine

To visualize axons from the CST, anterograde axonal tracing with biotin dextran amine (BDA) (Molecular Probes, Inc., Eugene, OR) was performed 12 weeks after the second operation after completion of the behavior analysis. Two or three animals in each of the six subgroups were randomly selected for BDA injection. Under deep anesthesia with 2% halothane with 1:2 nitrous oxide to oxygen, a craniotomy was performed to expose the sensorimotor cortex bilaterally, and 10% BDA dissolved in sterile water was injected at 12 sites in each sensorimotor cortex with a glass micropipette attached to a 26G needle (Becton, Dickinson and Co., Franklin Lakes, NJ) and a Picospritzer (General Valve Co., Fairfield, NJ) as previously reported (54). At each coordinate, 2 μ l of BDA was injected at a depth of 1.2 mm from the surface of the cortex. Then the skin was closed with 6-0 Vicryl. Animals were allowed to survive for 2 more weeks before they were sacrificed. Before the end of the planned period, three animals died within 2 weeks of BDA injection, and the spinal cords were removed and immersed in 10% neutral formalin within 12 hours of death for paraffin-embedded sections and histological examination.

Control GFP-PNs

One GFP transgenic Wistar rat was perfused with 4% paraformaldehyde (described in "Tissue Preparation") and 10 intercostal nerves were harvested to obtain axon counts. The bundle of 10 intercostal nerves

was placed in the chitosan channel and immersed in chilled universal fixative (1.16 g sodium phosphate monobasic, 0.27 g sodium hydroxide, 86 ml distilled water, 10 ml 40% formalin, and 4 ml 25% glutaraldehyde).

Tissue Preparation

At 14 weeks after the second operation, the rats were deeply anesthetized by an intraperitoneal injection of 1.0 ml of sodium pentobarbital. After an intracardiac injection of 1 ml of 1000 U/ml heparin, the animals were perfused through the ascending aorta with 500 ml of 4% paraformaldehyde in 0.1 mol/l phosphate buffer. A 2-cm length of spinal cord encompassing the implanted channel or compression site was carefully removed. The spinal cords from rats not injected with BDA were randomly allocated for histochemistry of paraffin-embedded sections or axon counts. The spinal cords from BDA-injected rats were used for histochemistry of frozen sections. The spinal cords for paraffin embedding were postfixed in 10% neutral buffered formalin for 3 days, then embedded in paraffin, after which 8 μ m-thick parasagittal sections were cut in a 1:8 series and mounted on Superfrost Plus slides (Fisher Scientific, Markham, Canada) or Platinum Line slides (W. Knittel, Braunschweig, Germany). The chitosan channels became very fragile in 10% neutral buffered formalin, and the channel walls were fragmented during sectioning of paraffin-embedded tissues. Accordingly, these sections usually showed empty segments at the location of the channel walls, and fragments of the disrupted channels were seen. Every eighth section was stained with Luxol Fast Blue (LFB) with hematoxylin and eosin (HE). Each paraffin section of that series was then prepared for immunohistochemistry as described in "Immunohistochemistry of Paraffin-fixed Tissue." The spinal cords for frozen sections were cryoprotected with 30% sucrose in 0.1 mol/l phosphate-buffered saline (PBS) at 4°C, then frozen and embedded in Frozen Section Medium compound (Stephens Scientific, Riverdale, NJ). Twenty μ m-thick parasagittal sections were cut in a 1:6 series on a cryostat and mounted on cold (-20°C) Platinum Line microscope slides. The spinal cords for axon counts were preserved in universal fixative for 2 weeks and sectioned as described in "Axon Counts and Measurements."

Immunohistochemistry

The following antibodies were used for the immunohistochemical assessments: mouse antineurofilament 200 monoclonal antibody (NF200) 1:400 dilution in paraffin sections and 1:500 in frozen sections (Sigma, St. Louis, MO) to visualize neurons and axons; mouse antigial fibrillary acidic protein monoclonal antibody (GFAP) 1:200 (Boehringer-Mannheim Chemicon, Temecula, CA) to visualize astrocytes; mouse antirat 192 IgG p75NTR monoclonal antibody (p75) 1:100 (gift from Dr. Phil Baker, Montreal Neurological Institute, McGill University, Montreal, Canada) to visualize Schwann cells; mouse antirat protein 0 monoclonal antibody (P0) 1:300 (provided by Dr. Juan Archelos, Department of Neurology, University of Graz, Graz, Austria) to visualize peripheral myelin produced by Schwann cells (1); rat anticalcitonin gene-related peptide polyclonal antibody (CGRP) 1:3000 (Immunostar, Hudson, WI) to visualize sensory axons from dorsal root ganglia (DRG); rabbit anti-green fluorescent protein polyclonal antibody (GFP) 1:500 (Abcam, Inc., Cambridge, MA) to visualize GFP; mouse anti-CC1/APC monoclonal antibody (CC1) 1:1000 (Calbiochem, San Diego, CA) to visualize oligodendrocytes; mouse antirat monocytes/macrophages monoclonal antibody (ED-1) 1:500 (Serotec, Raleigh, NC) to visualize activated macrophages; mouse anti-smooth muscle actin monoclonal antibody (SMA) 1:100 (DAKO, Mississauga, Canada) to visualize blood vessels; and mouse anti-Ki67 liquid antibody (Ki67) 1:200 (Clone MM1; Novocastra, Burlington, Canada) to visualize proliferating cells. In all

the immunohistochemistry procedures, appropriate negative controls were used with the omission of the primary antibodies.

Immunohistochemistry of Paraffin-fixed Tissue

For immunohistochemistry of paraffin-embedded sections, anti-NF200, GFAP, P0, GFP, ED-1, SMA, and Ki67 antibodies were used. The sections for GFAP and Ki67 were pretreated with 1% H₂O₂ in methanol for 30 minutes at room temperature (RT) to reduce nonspecific staining by endogenous peroxidases. The slides for Ki67 were placed in a pressure cooker with 3 g/l sodium citrate buffer (pH 6.0) and heated in a microwave for 30 minutes on high power. To expose antigen sites, the slides for SMA were placed in a pressure cooker with 10 nmol/l Tris buffer and 1 mmol/l ethylenediaminetetraacetic acid at pH 9.0 and heated in a microwave for 30 minutes on high power. After heating, the slides were left in the microwave for another 30 minutes for cooling. For NF200, a plastic coplin jar filled with a solution of ethylenediaminetetraacetic acid at pH 8.0 buffer was heated in a steamer for 30 minutes. The slides were then placed in the ethylenediaminetetraacetic acid buffer in the coplin jar and heated in the steamer for 30 minutes and were then left for 20 minutes for cooling. After rinsing with PBS, all sections except for Ki67 were blocked for nonspecific antibody binding at RT for 1 hour with the following: 10% heat-inactivated goat serum in PBS containing 0.3% Triton X-100 for GFAP, NF200, and P0; 4% normal goat serum (NGS) in PBS containing 0.1% Triton X for ED-1 and SMA; and 3% NGS in 0.1% bovine serum albumin (1 ml NGS, 0.033 g bovine serum albumin, and 32.2 ml SPBS) for GFP. The sections for Ki67 were blocked for nonspecific antibody at RT for 10 minutes with 2% normal horse serum in PBS containing 0.3% Triton X. After the above steps, all sections except those for Ki67 were incubated overnight in a solution of primary antibody diluted in blocking solutions at 4°C. After being washed three times with PBS, the specimens were incubated with biotinylated antimouse IgG (H+L) antibody (Vector Laboratories, Burlingame, CA) 1:500 dilution in PBS for NF200, GFAP, P0, ED-1, SMA, and Ki67 and antirat IgG (H+L) goat antirabbit antibody for GFP. The sections were then washed three times in PBS and incubated with avidin-biotin peroxidase complex (Vectostain ABC Kit Standard; Vector Laboratories) for peroxidase staining and visualization with diaminobenzidine tetrahydrochloride (Vector Laboratories). The sections were coverslipped with Entellan (EM Science, Gibbstown, NJ), then observed under a Leica DMRBlight microscope (Leica, Nussloch, Germany) and photographed using an image tiling and stitching system on Stereo Investigator (MicroBrightField Bioscience, Williston, VT).

Immunohistochemistry of Frozen Tissue and Visualization of Biotin Dextran Amine

For immunohistochemistry of frozen sections, anti-NF200, p75, CGRP, GFAP, and CC1 antibodies were used. Sections were thawed and washed three times with PBS for 10 minutes. For NF200 or GFAP, sections were pretreated as described above. The sections for CGRP were pretreated with 1% H₂O₂ in methanol for 10 minutes at RT. After being rinsed with PBS, the sections were blocked for nonspecific antibody binding at RT for 1 hour with the following: 10% heat-inactivated goat serum in PBS containing 0.3% Triton X-100 for GFAP and NF200; 10% NGS for p75; and 2% NGS containing 0.3% Triton X-100 for CC1. Then, all sections were incubated overnight in a solution of primary antibody diluted in blocking solutions at 4°C. After being washed three times with PBS, the specimens were incubated with Alexa Fluor 488 goat antimouse and goat antirabbit IgG (H+L) conjugate highly cross-absorbed (1:500 dilution in PBS) (Molecular Probes, Inc.) for 1 hour. The sections were counterstained with the nuclear dye 4',6-diamidino-2-phenylindole and coverslipped.

Every sixth slide in the series of frozen sections was selected for BDA detection. After being washed with 0.1 mol/l PBS, these sections were pretreated with 1% H₂O₂ in methanol for 10 minutes at RT. After being rinsed with PBS containing 0.5% Triton X for 30 minutes, the slides were incubated in avidin-biotin peroxidase complex (Vectostain Elite ABC Kit Standard; Vector Laboratories) for 1 hour at RT. The slides were washed twice with PBS, then Alexa Fluor 488 was applied for 1 hour at RT. After being rinsed three times with PBS, the sections were mounted and coverslipped.

All sections were examined and photographed using a Zeiss-LSM 510 confocal microscope (Zeiss, Oberkochen, Germany). Z-stack images were accumulated based on 20 to 30 optical sections, at 0.5 μm in thickness per section. Then the entire thickness of the section was visualized using the ImageJ software system (National Institutes of Health, Bethesda, MD). Three-dimensional imaging was constructed using Imaris software (Bitplane, Exton, PA).

Transmission Electron Microscopy

Four animals (n = one per group in Groups SA+C+PN, CH+C+PN, SA+EC, and CH+EC) were randomly selected for transmission electron microscopy. Fourteen weeks after channel implantation or no channel, animals were sacrificed by intraperitoneal injection of sodium pentobarbital and transcardially perfused using 2% paraformaldehyde with 2.5% glutaraldehyde in 0.1 mol/l sodium cacodylate buffer. The implanted channel was removed from the spinal cord and transected at the midpoint in the dorsoventral plane. There was no tissue bridge inside the channels in Groups SA+EC and CH+EC; therefore, sections for transmission electron microscopy were performed on one animal from Group SA+C+PN and one animal from Group CH+C+PN. The dissected tissue inside the channel was postfixed in 1% osmium tetroxide. The samples were then washed for 10 minutes in sodium cacodylate three times followed by quick washes with 0.1 mol/l acetate buffer, and the tissue stained with 1% uranyl acetate overnight at 4°C. The tissue was washed again with acetate buffer and progressively dehydrated with increasing ethanol concentrations from 50 to 100% for 10 minutes each. After an additional 2 to 10 minutes, the tissue was washed with 100% ethanol, followed by two quick washes with propylene oxide, then the samples were infiltrated and embedded in Araldite resin in inverted polyethylene capsules with the tips removed to allow overnight curing in a 60°C vacuum oven. Sections were cut at 0.5 μm and stained with 1% toluidine blue for orientation, then thin sections of approximately 90 nm were made with a Reichert-Jung Ultratuc E ultramicrotome (Reichert-Jung, Vienna, Austria), mounted on copper mesh grids and counterstained with uranyl acetate and lead citrate for 5 minutes each. The grids were viewed and photographed with a Hitachi H7000 transmission electron microscope (Hitachi, Tokyo, Japan).

Axon Counts and Measurements

For axon counts and measurements, four animals in each of Groups SA+C+PN, CH+C+PN, SA+EC, and CH+EC were randomly chosen, a 2-cm segment of spinal cord encompassing the implanted channel was removed and immersed in universal fixative for 2 weeks, and a 1-mm-thick slice of the channel was prepared. There was no tissue bridge in two of four animals in Group SA+EC or in any of the four animals in Group CH+EC; therefore, they were excluded. The 1-mm slice containing the middle portion of the tissue bridge in the rostrocaudal direction was embedded in resin, then sectioned at 1-μm thickness. A 1-mm segment of a nonimplanted channel containing 10 intercostal nerves prepared as described above was also embedded in resin, then sectioned at 1-μm thickness as a PN control. All 1-μm sections were stained with toluidine blue and examined under the Leica DMRB light

TABLE 2. Axon counts^a

Group	Bridge area, mm ²	No. of fibers	Fiber diameter, μm	Axon diameter, μm	Myelin thickness, μm	G ratio
1a	0.369 ± 0.093	35,260 ± 10,590	3.034 ± 0.090	1.630 ± 0.123	0.700 ± 0.056	0.547 ± 0.036
2a	0.359 ± 0.091	25,590 ± 10,440	2.651 ± 0.574	1.270 ± 0.315	0.705 ± 0.143	0.480 ± 0.043
1a	0.162 ± 0.007	649.6 ± 336.1	4.888 ± 0.803	2.530 ± 0.555	1.180 ± 0.200	0.515 ± 0.050
PN control	1.369 ± 0.821	50,070 ± 27,860	7.009 ± 0.248	3.712 ± 0.158	1.649 ± 0.079	0.530 ± 0.014

^a Bridge area, area of the tissue bridge in cross section; No. of fibers, total number of myelinated fibers in channel; G ratio, ratio of axon diameter to fiber diameter. Values shown are mean ± standard error of the mean.

microscope. Five 1-μm sections per animal were randomly selected, and the area occupied by tissue in each section was measured. Seven photographs of high-power fields (1446 μm² at ×1000 magnification) were taken randomly from each section and without overlap, and myelinated fibers greater than 0.5 μm in diameter were counted and averaged to obtain the number of myelinated fibers in the seven photographs. Using the average number of myelinated fibers and the area of each section occupied by tissue, the total number of myelinated fibers in each section was calculated. The color intensity-based method with the aid of Image Pro-Plus software (Media Cybernetics, Silver Spring, MD) was used to identify and measure the following parameters of healthy myelinated axons in HPF pictures: 1) the total area encompassed by the entire cross section of the bridging tissue in the channel; 2) the total number of axons in the channel, calculated by the axon density and the dimension of the whole bridging tissue (*fiber* is defined as the combination of axon and myelin); 3) the entire fiber diameter and area; 4) the axon diameter and area (*axon* indicates the axonal component, excluding myelin, of the myelinated fiber); 5) the thickness of myelin; 6) the G ratio, i.e., the ratio of axon diameter to entire fiber diameter; and 7) the frequency distribution of fibers of varying size. The histograms for 1 to 6 and line graph for 7 were made using Sigma Plot 8.0 for Windows (Systat Software, Inc., San Jose, CA). The total number of axons analyzed for each of these parameters is shown in *Table 2*.

Channel Wall Thickness

The thickness of the wall of the channels at 14 weeks was measured and compared with that of nonimplanted channels. After preparation of the tissue for the axon counts described above, the remaining segments of the channels were preserved in 30% sucrose (n = 16) for 3 days, then sectioned transversely in a cryostat at 20 μm, and mounted on Superfrosted Plus slides without coverslipping. For comparison, three nonimplanted channels were preserved in universal fixative for 2 weeks, then in 30% sucrose for 3 days, then sectioned transversely and mounted. The channel wall thickness was measured using Bioquant Imaging Software (R&M Biometrics, Inc., Nashville, TN). In each section, 24 samples of the channel wall were randomly selected without overlap and measured (a total of 384 sites in 16 implanted channels and 72 sites in three nonimplanted channels).

Measurement of Cavity Length in the Injured Spinal Cord

Measurement of the cavity length after clip injury was determined in LFB/HE-stained paraffin-embedded parasagittal sections. The section containing the longest cavity in the no-channel groups was selected, and the cavity was measured using Bioquant Imaging Software.

Statistics

Data from more than two groups were analyzed by one-way analysis of variance. The differences between two groups were analyzed by Student’s *t* test. The BBB score was analyzed by one-way repeated-measures analysis of variance. Statistical analysis was performed using Sigma Plot 8.0 for Windows and Microsoft Excel 2000 (Microsoft Corp., Seattle, WA).

RESULTS

Implanted Channels Showed No Degradation at 14 Weeks

Fourteen weeks after implantation, the channels remained concentric, with no visible degradation (*Fig. 2*). There was no significant difference in the thickness of the walls before (219 ± 27.9 μm, n = 3) and after (207 ± 62.8 μm, n = 16; subacute, n = 8, and chronic, n = 8 groups) implantation (*P* = 0.405, Student’s *t* test).

Implanted Channels Produced Minimal Tissue Reaction in the Spinal Cord at 14 Weeks

There was minimal inflammatory reaction at the interface between the spinal cord and the channels at 14 weeks. There were only a few macrophages along the walls of the channels and minimal astrocytic or fibrotic reaction (*Figs. 3–5*).

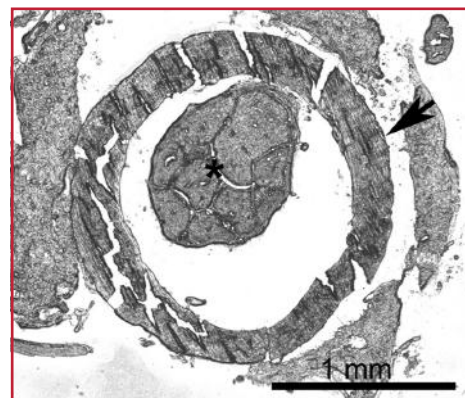
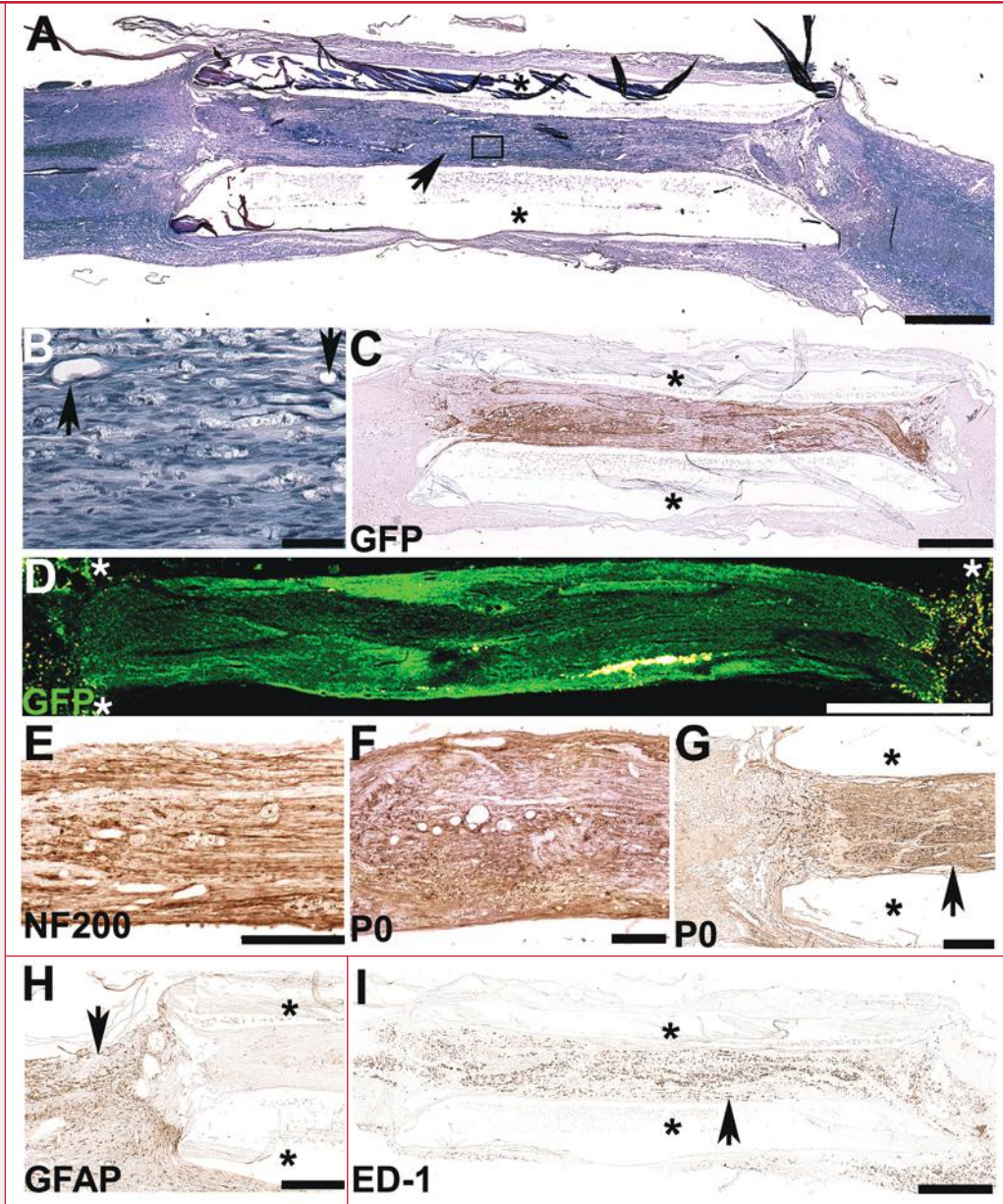


FIGURE 2. Twenty-μm cross-section of the intramedullary chitosan channel (arrow) containing a tissue bridge (asterisk) at 14 weeks after chronic implantation of the channel + PN grafts.

FIGURE 3. Twenty- μm parasagittal paraffin sections (A–C, E–I) and frozen section (D) 14 weeks after chronic implantation of the channel containing PN grafts. The majority of the channels disintegrated during sectioning of paraffin-embedded tissues; therefore, there are two linear spaces corresponding to the remnants of the channel walls containing fragments of the channels (asterisks in A, C, D, G–I). D, the tissue bridge from a non-stained frozen section under a green and red filter and the images were merged. In each panel, rostral is on the left. A and B, Luxol Fast Blue (LFB)/hematoxylin and eosin (HE)-stained sections. A, a thick tissue bridge is shown between the channel walls (arrow in A). B, the boxed area in A is shown at a higher power in B; there are many Schwann cells with elongated nuclei accompanied by blue myelin arranged in a parallel fashion. Blood vessels are shown (arrows). C, GFP-immunostained sections; the majority of the GFP-positive cells are localized within the tissue bridge, and no GFP-positive cells are observed in the spinal cord adjacent to the tissue bridge. D, GFP-positive cells are also clearly detected with fluorescent microscopy. Note that autofluorescence and bloodborne cells (presumably macrophages) are detected in yellow. Mouse antineurofilament 200 monoclonal antibody (NF 200)–(E) and mouse antirat protein 0 monoclonal antibody (P0)–(F) immunostained sections from the center of the tissue bridge; many NF200-positive axons are seen in the bridge (E). G and H, peripheral myelin immunolabeled with P0 is also observed in the bridge; P0 (G) and mouse antiglial fibrillary acidic protein monoclonal antibody (GFAP) (H) immunostained sections from the rostral end of the bridge. G, The majority of P0-immunopositive peripheral myelin is localized within the bridge (arrow). H, GFAP-immunostaining shows a distinct margin between the tissue bridge and the spinal cord adjacent to the tissue bridge (arrow) owing to a dense accumulation of reactive astrocytes in the spinal cord. I, mouse antirat monocytes/macrophages monoclonal antibody (ED-1)-immunostained sections: large aggregations of ED-1-positive macrophages/microglia are present in the bridges (arrow) and adjacent spinal cord; however, no aggregations of macrophages are found in the channel walls. Scale bars, 1 mm (A, C, D, and I); 100 μm (B and E); 500 μm (F–H).



Implanted Channels with PN Grafts Had Tissue Bridges Containing a Large Number of Regenerated Axons after Subacute or Chronic Implantation

Parasagittal sections stained with LFB/HE showed a thick tissue bridge in the PN-filled channels in all animals in the subacute and chronic groups (Fig. 3A). The bridges contained

many Schwann cells accompanied by myelinated fibers stained blue with LFB and blood vessels (Fig. 3B). The tissue bridges contained numerous GFP-positive cells (Fig. 3, C and D), large numbers of NF200-positive axons (Fig. 3E), and P0-positive peripheral myelin produced by Schwann cells (Fig. 3, F and G). Previous studies from our laboratory on transplantation of

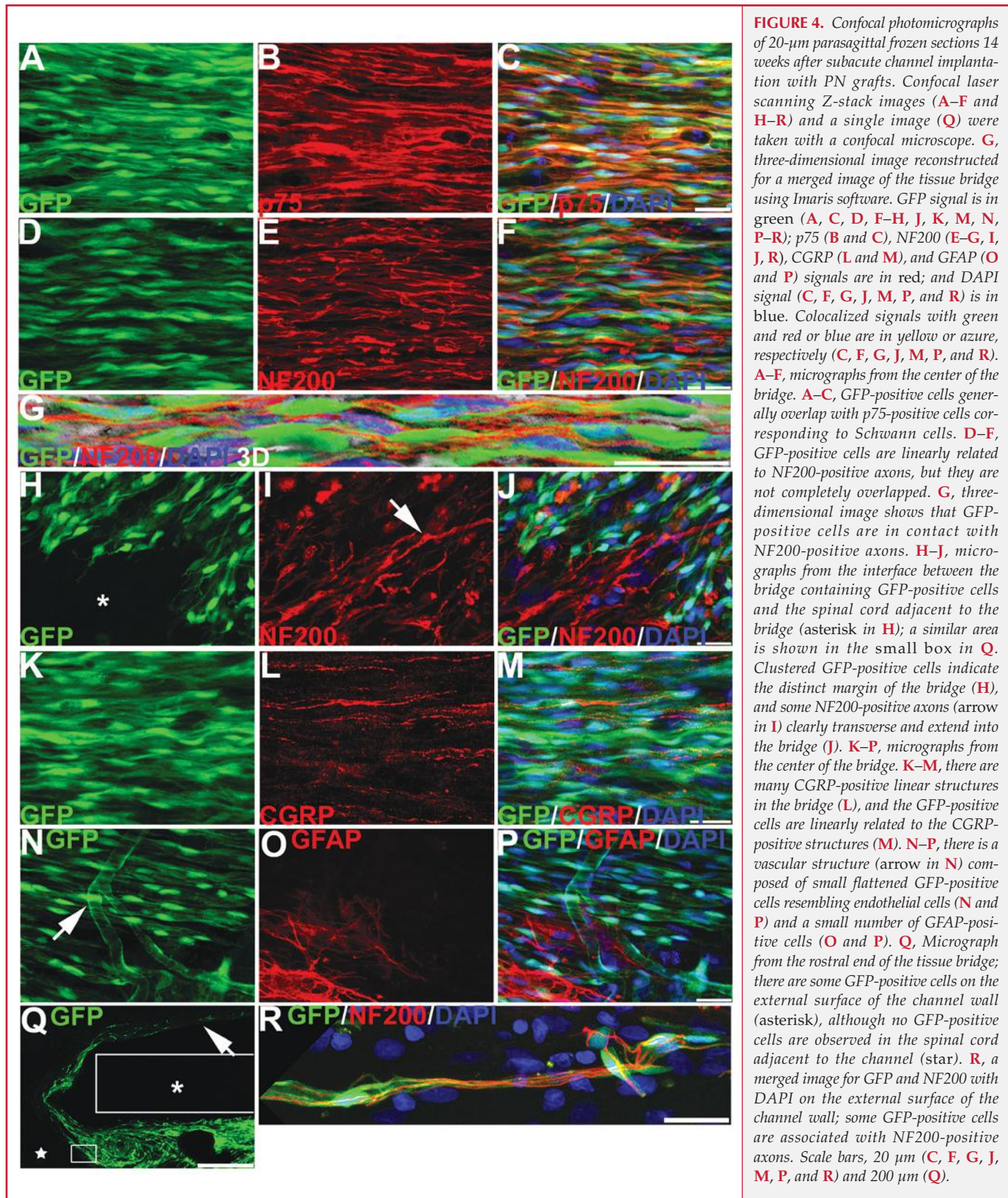


FIGURE 4. Confocal photomicrographs of 20- μ m parasagittal frozen sections 14 weeks after subacute channel implantation with PN grafts. Confocal laser scanning Z-stack images (**A–F** and **H–R**) and a single image (**Q**) were taken with a confocal microscope. **G**, three-dimensional image reconstructed for a merged image of the tissue bridge using Imaris software. GFP signal is in green (**A**, **C**, **D**, **F–H**, **J**, **K**, **M**, **N**, **P–R**); p75 (**B** and **C**), NF200 (**E–G**, **I**, **J**, **R**), CGRP (**L** and **M**), and GFAP (**O** and **P**) signals are in red; and DAPI signal (**C**, **F**, **G**, **J**, **M**, **P**, and **R**) is in blue. Colocalized signals with green and red or blue are in yellow or azure, respectively (**C**, **F**, **G**, **J**, **M**, **P**, and **R**). **A–F**, micrographs from the center of the bridge. **A–C**, GFP-positive cells generally overlap with p75-positive cells corresponding to Schwann cells. **D–F**, GFP-positive cells are linearly related to NF200-positive axons, but they are not completely overlapped. **G**, three-dimensional image shows that GFP-positive cells are in contact with NF200-positive axons. **H–J**, micrographs from the interface between the bridge containing GFP-positive cells and the spinal cord adjacent to the bridge (asterisk in **H**); a similar area is shown in the small box in **Q**. Clustered GFP-positive cells indicate the distinct margin of the bridge (**H**), and some NF200-positive axons (arrow in **I**) clearly transverse and extend into the bridge (**J**). **K–P**, micrographs from the center of the bridge. **K–M**, there are many CGRP-positive linear structures in the bridge (**L**), and the GFP-positive cells are linearly related to the CGRP-positive structures (**M**). **N–P**, there is a vascular structure (arrow in **N**) composed of small flattened GFP-positive cells resembling endothelial cells (**N** and **P**) and a small number of GFAP-positive cells (**O** and **P**). **Q**, Micrograph from the rostral end of the tissue bridge; there are some GFP-positive cells on the external surface of the channel wall (asterisk), although no GFP-positive cells are observed in the spinal cord adjacent to the channel (star). **R**, a merged image for GFP and NF200 with DAPI on the external surface of the channel wall; some GFP-positive cells are associated with NF200-positive axons. Scale bars, 20 μ m (**C**, **F**, **G**, **J**, **M**, **P**, and **R**) and 200 μ m (**Q**).

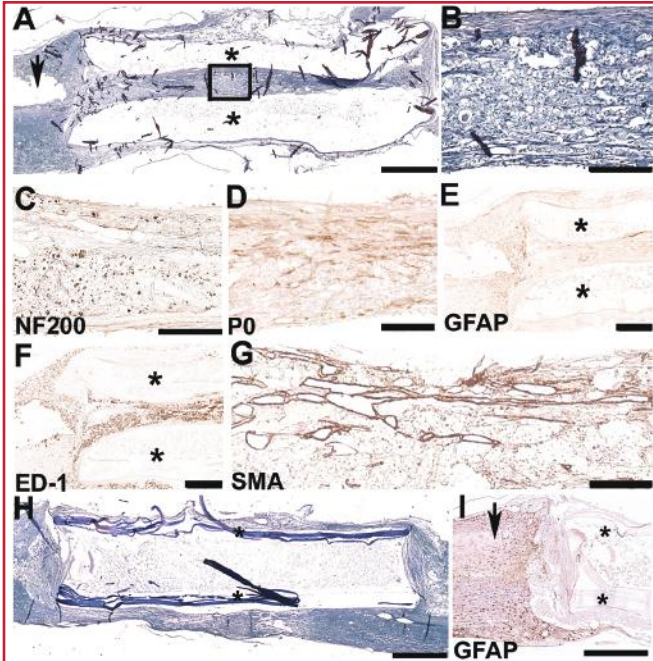


FIGURE 5. Twenty- μm parasagittal paraffin sections 14 weeks after implantation of empty channels after subacute (A–G) and chronic (H and I) implantation. There are two spaces corresponding to the remnants of the channel walls associated with fragments of the disrupted channels (asterisks in A, E, F, H, and I). In each panel, rostral is on the left. A and B, LFB/HE stained section; there is a tissue bridge in the channel smaller than in Figure 3. A cavity in the rostral spinal cord adjacent to the bridge is seen (arrow in A). The boxed area in A is shown at a higher power in B. There were many macrophages containing debris of the central myelin stained in green; however, Schwann cells accompanied by myelinated structures in blue were not prominent. NF200- (C) and P0- (D) immunostained sections at the center of the bridge; sparse NF200-positive axons (C) and peripheral myelin immunolabeled with P0 (D) are compared with Figure 3. (E) GFA-immunostained sections. GFAP-immunostaining shows a dense accumulation of reactive astrocytes in the rostral spinal cord adjacent to the bridge. F, ED-1-immunostained section; there is a significant aggregation of ED-1-positive macrophages in the bridge and spinal cord, although there is no accumulation of macrophages in the channel walls. (G) SMA-immunostained section; many blood vessels immunolabeled with SMA are seen in the bridge. H, LFB/HE-stained section; there is no tissue bridge in the channel after chronic implantation of an empty channel, and the channel contains macrophages and cellular debris. I, GFAP-immunostained sections; a dense accumulation of GFAP-positive astrocytes is seen in the rostral spinal cord adjacent to the channel (arrow). Scale bars, 1 mm (A, H, and I), 200 μm (B–D and G), and 500 μm (E and F).

peripheral nerve grafts into the transected spinal cord (50) revealed the complete absence of NF200-staining structures in the grafts as early as 2 weeks after transplantation, indicating that all of the grafted axons had completely degenerated. Thus, all NF200 structures in the grafts in the present study represent regenerated or sprouted axons. GFAP immunostaining showed a dense accumulation of reactive astrocytes in the spinal cord

adjacent to the tissue bridges (Fig. 3H). Large aggregations of ED-1-positive macrophages/microglia were present in the tissue bridges and adjacent spinal cord. However, there were no aggregations of macrophages in or along the channel walls (Fig. 3I). SMA immunostaining showed a large number of blood vessels in the tissue bridges (data not shown). There were no Ki67-positive cells in the tissue bridges (data not shown). Confocal microscopy revealed many GFP-positive cells arranged longitudinally in the tissue bridges (Fig. 4, A, C, D, F–H, J, K, M, N, and P) with bipolar processes and elongated nuclei labeled with 4',6-diamidino-2-phenylindole. Immunohistochemistry showed that the GFP-positive cells were morphologically identical to p75-positive Schwann cells (Fig. 4, A–C), were arranged longitudinally in relationship to adjacent NF200-positive axons (Fig. 4, D–F), and three-dimensional images showed that these cells were in contact with axons (Fig. 4G). No GFP-positive cells migrated into the rostral or caudal spinal cord adjacent to the tissue bridges (Figs. 3, C and D, and 4, H and J); thus, there was a sharp demarcation between the tissue bridge containing GFP-positive cells and the spinal cord adjacent to the tissue bridge. However, some NF200-labeled axons penetrated across the cord-bridge interface into the tissue bridge (Fig. 4, H–J). There were numerous CGRP-positive fibers adjacent to the GFP-positive cells in the tissue bridges (Fig. 4, K–M). Confocal microscopy revealed many vascular structures lined by small flattened GFP-positive endothelial cells in the tissue bridges (Fig. 4, N–P). A small number of GFAP-positive cells, presumably astrocytes, was found in the bridges (Fig. 4, N–P). Interestingly, there was a small number of GFP-positive Schwann cells on the external surface of the channel walls, and migrating GFP-positive cells could be followed as they exited the channels and migrated along the external surface of the channel walls (Fig. 4Q). These cells were spatially related to NF200-positive axons outside of the channels, suggesting axonal myelination by the cells (Fig. 4R). No CC1-positive cells were found in the tissue bridges (data not shown). There were no BDA-labeled fibers in the tissue bridges or caudal spinal cord, although BDA-labeled fibers were detected in the spinal cord rostral to the bridges. Multiple cavities were present in the adjacent spinal cord rostral and caudal to the tissue bridges.

Transmission electron microscopy of the tissue bridges showed numerous myelinated axons (Fig. 6, A and B). Most of the axons were myelinated by Schwann cells identified by their basal lamina (Fig. 6C), although there were some nonmyelinated axons (Fig. 6D). There was a small number of fibroblasts with dilated endoplasmic reticulum producing collagen in the tissue bridges. Overall, there were no histological differences between PN-filled channels implanted in the subacute (Group SA+C+PN) and chronic (Group CH+C+PN) groups.

Empty Channels Produced Small Tissue Bridges after Subacute, but Not Chronic, Implantation

Animals implanted with unfilled channels showed major differences compared with the PN-filled channels. There was a tissue bridge in only two of the five subacute animals in Group SA+EC (Table 1, paraffin and frozen sections), and no

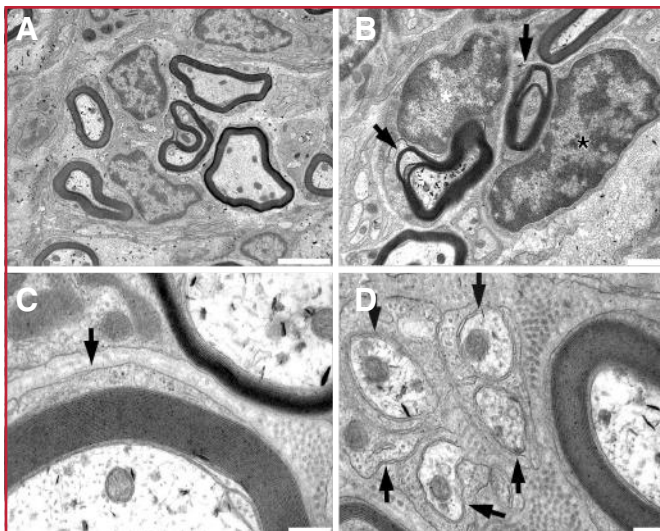


FIGURE 6. Transmission electron microscopy of tissue bridges 14 weeks after chronic implantation of a channel with PN grafts. **A**, many myelinated fibers and Schwann cells are seen. **B**, each Schwann cell (asterisks) is related to one myelinated fiber (arrows). **C**, a myelinated fiber is contained within a Schwann cell surrounded by a basal lamina (arrow), characteristic of Schwann cells. **D**, several nonmyelinated axons (arrows) are also seen. Scale bars, 2 μm (**A**), 1 μm (**B**), 0.2 μm (**C**), and 0.5 μm (**D**).



FIGURE 7. Twenty- μm parasagittal paraffin section stained with LFB/HE 14 weeks after no channel implantation in subacute group. There are multiple large cavities in the damaged spinal cord. Scale bar, 1 mm.

tissue bridge in the other three (Fig. 5A). LFB/HE-stained sections showed many macrophages containing debris, especially central myelin-stained green. These bridges contained only a small number of Schwann cells and myelinated fibers stained blue with LFB (Fig. 5B), a small number of NF200-positive fibers (Fig. 5C), and some P0-positive peripheral myelin (Fig. 5D). There were many GFAP-positive astrocytes in the spinal cord adjacent to the tissue bridges and a few astrocytes in the tissue bridge (Fig. 5E). There were large aggregations of ED-1-positive macrophages in the tissue bridges and adjacent spinal cord, but no aggregation of macrophages along the channel walls (Fig. 5F). SMA-immunostaining showed many blood vessels in the tissue bridges (Fig. 5G). Multiple cavities were present in the spinal cord adjacent to the unfilled channels. In contrast, there was no tissue bridge in the unfilled channels in any of the chronic implantation animals (Group CH+EC, Fig. 5H), and there was a dense accumulation of GFAP-positive astrocytes in the adjacent rostral and caudal

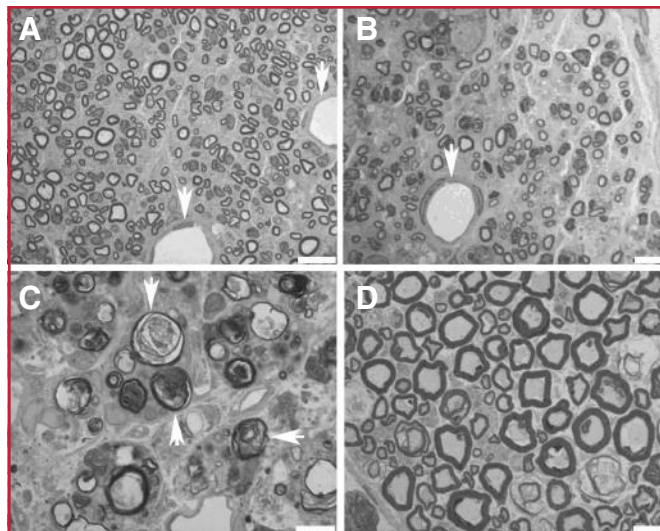


FIGURE 8. One- μm cross-sections 14 weeks after channel implantation with PN grafts after subacute (Group SA+C+PN) (**A**) and chronic implantation (Group CH+C+PN) (**B**), empty channel implantation for subacute SCI (Group CH+C+PN) (**C**), and a nonimplanted control channel containing 10 intercostal nerves (PN control) (**D**). **A** and **B**, numerous myelinated fibers and some blood vessels (arrows) are seen. **C**, some axons are severely ballooned and degenerated (arrows). **D**, numerous dense myelinated fibers are seen. The subacute channel group showed more axons than the chronic group, but the axons were generally smaller than those in the PN control. Scale bars, 10 μm .

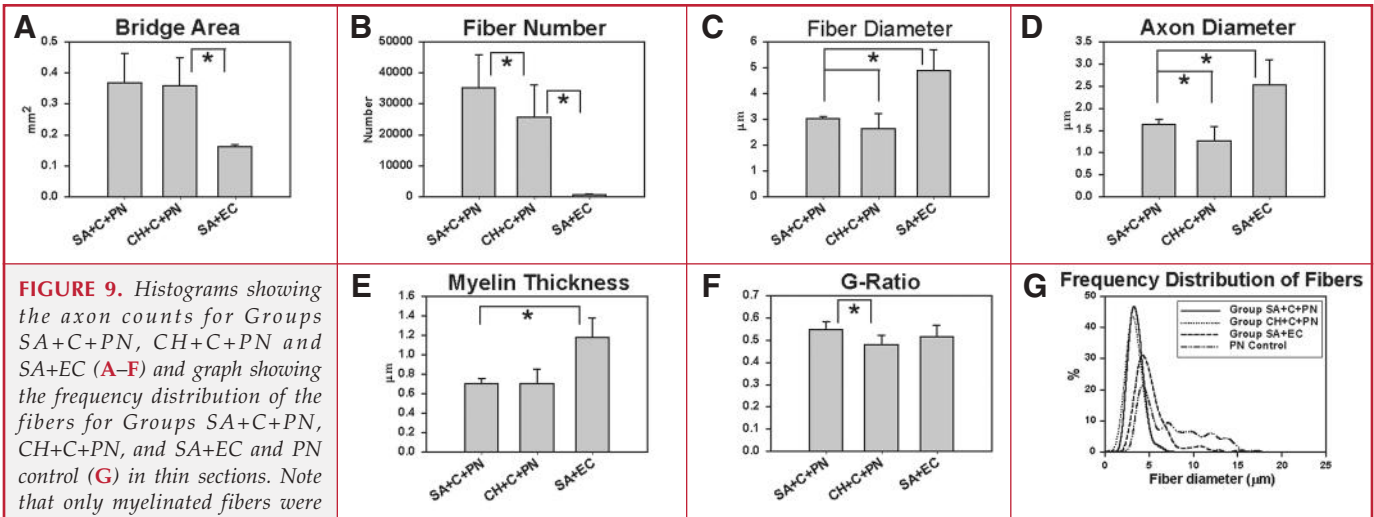
spinal cord (Fig. 5I). There were no BDA-labeled fibers in the caudal spinal cord in Group SA+EC and CH+EC rats.

No-channel Groups Had Large Cavities

LFB/HE-stained sections showed multiple large cavities in the spinal cord at the injury site in the no-channel subacute (Group SA+N) and chronic (Group CH+N) groups (Fig. 7), and there was no significant difference in the length of the cavities at 14 weeks in the subacute (8.5 ± 2.5 mm, $n = 10$) or chronic (8.9 ± 2.4 mm, $n = 11$) groups ($P = 0.81$). There were no NF200-positive axons traversing the injury site, and there was a massive accumulation of GFAP-positive astrocytes and aggregations of ED-1-positive macrophages in the adjacent spinal cord. A small number of P0-positive cells was observed near the epicenter of the damaged cord. There were no BDA-labeled fibers in the caudal spinal cord.

Axon Counts Showed Numerous Myelinated Fibers in the Tissue Bridges

Thin sections revealed large numbers of myelinated fibers and blood vessels in the tissue bridges after implantation of PN-filled channels after subacute (Group SA+C+PN) or chronic (Group CH+C+PN) implantation (Fig. 8, A and B). There was a small number of myelinated fibers in the unfilled channels in the subacute animals (Group SA+EC), although the size of the fibers varied considerably, and some axons were severely bal-

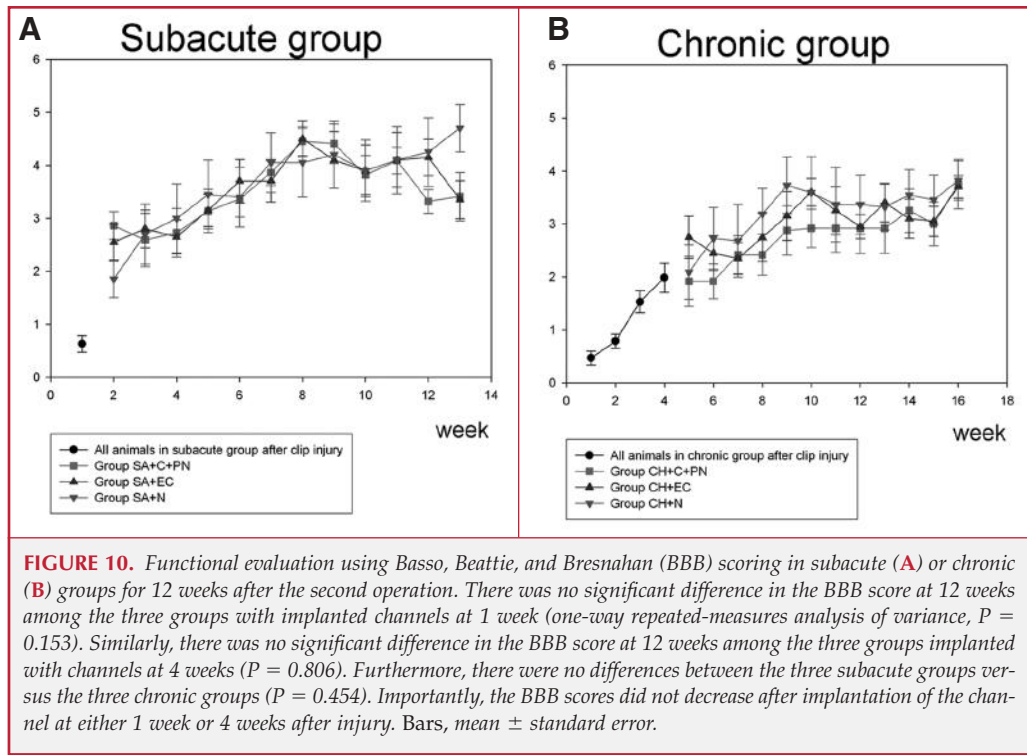


looned and degenerated (Fig. 8C). In the PN graft control (PN control), the fibers were larger than those in Groups SA+C+PN and CH+C+PN at 14 weeks (Fig. 8D). As noted above, there were no bridges in the channels in Group CH+EC. The cross-sectional area in the channel occupied by the tissue bridges in Groups SA+C+PN and CH+C+PN was significantly greater than that of Group SA+EC ($P < 0.05$) (Fig. 9A). The total number of myelinated fibers was $35,260 \pm 10,590$ in Group SA+C+PN, $25,590 \pm 10,440$ in Group CH+C+PN, and 649.6 ± 336.1 in Group SA+EC. There was a significant difference between Groups SA+C+PN and CH+C+PN ($P = 0.006$) (Fig. 9B), demonstrating greater axonal regeneration in the subacute group. The fiber diameter was significantly larger in Group SA+C+PN ($3.034 \pm 0.090 \mu\text{m}$) than that in Group CH+C+PN ($2.651 \pm 0.574 \mu\text{m}$) ($P = 0.007$) (Fig. 9C). Also, the axon diameter in Group SA+C+PN ($1.63 \pm 0.12 \mu\text{m}$) was significantly larger than that in Group CH+C+PN ($1.27 \pm 0.32 \mu\text{m}$) ($P < 0.001$) (Fig. 9D). In contrast, there was no significant difference in myelin thickness between Group SA+C+PN ($0.700 \pm 0.056 \mu\text{m}$) and Group CH+C+PN ($0.705 \pm 0.143 \mu\text{m}$) ($P = 0.285$) (Fig. 9E). The G ratio, i.e., the ratio of axon diameter to fiber diameter, was significantly different between Group SA+C+PN (0.547 ± 0.036) and Group CH+C+PN (0.480 ± 0.043) ($P < 0.001$) (Fig. 9F).

The cross-sectional area and frequency distribution of fiber diameter of the PN control were compared with the tissue bridges in Groups SA+C+PN, SA+EC, and CH+C+PN (Table 2). The area occupied by the grafts was calculated as a percentage of the area of the channel lumen in Groups SA+C+PN, CH+C+PN, and SA+EC and was 26.2, 27.0, and 11.8%, respectively, compared with that in the PN control. In addition, the fiber diameter in Groups SA+C+PN and CH+C+PN was significantly smaller than that in the PN control ($7.009 \pm 0.248 \mu\text{m}$) ($P < 0.001$), which contained a large number of myelinated fibers ($50,070 \pm 27,860$) (Table 2). Interestingly, the distribution of fiber diameter showed a peak between 2 and 5 μm (Fig. 9G), where the percentage of fiber diameters in this range was 88.2, 80.3, 69.0, and 40.7% in Groups SA+C+PN, CH+C+PN, and SA+EC and the PN control, respectively. Thus, the axons in Groups SA+C+PN and CH+C+PN were significantly smaller than those in the PN control. However, most of the fibers in all groups, including the PN control, were between 3 and 5 μm in fiber diameter, indicating that most of the regenerated fibers were similar to those in the PN control.

Functional Evaluation

There was no significant difference in the BBB score at 12 weeks among the three subacute groups treated at 1 week (Fig. 10A)



(one-way repeated measures analysis of variance, $P = 0.153$). Similarly, there was no significant difference in the BBB score at 12 weeks among the three chronic groups treated at 4 weeks (Fig. 10B, $P = 0.806$). Furthermore, there were no differences between the three subacute groups and the three chronic groups ($P = 0.454$). None of the animals achieved plantar placement of the paw with weight support, which corresponds to a BBB score of 9.

DISCUSSION

We describe a new spinal cord repair strategy for the severely damaged spinal cord based on intramedullary, intracavitary implantation of a novel chitosan channel containing PN grafts. Delayed implantation at 1 or 4 weeks after injury produced a thicker tissue bridge containing a larger number of myelinated axons and well developed blood vessels bridging the spinal cord compression site compared with empty channels.

Subacute versus Chronic Implantation

Repair of chronic SCI in the rodent is more difficult than repair of subacute SCI because of the massive glial scarring surrounding the lesion after 4 weeks. Although the role of reactive astrocytes after SCI is controversial (41), the glial scar, composed of reactive astrocytes and proteoglycans, likely inhibits axonal regeneration (7, 44). In the present study, the rats treated in the subacute stage (1 wk) had more axons in the tissue bridge than the rats treated in the chronic stage (4 wk). Also, the bridges were larger in the channels containing PNs than in the empty channels, and no tissue bridges were present in the

chronic empty channel group. The glial scar adjacent to the tissue bridges may have acted as a physical or chemical barrier to axonal regeneration (Figs. 3–5). However, it is quite remarkable that we were able to induce an average of approximately 25,000 axons in the chronic group (Table 2).

Axonal Regeneration or Sprouting

The subacute PN-filled channel group had the largest number of myelinated fibers in the tissue bridge ($35,260 \pm 10,590$), although the chronic group also had a large number of axons ($25,590 \pm 10,440$). To our knowledge, these groups had the largest number of regenerated axons of any previous study of SCI treatment, including grafted Schwann cells (9, 11, 15, 21, 27, 34). For example, cultured Schwann cells transplanted into the cavity 1 week after mild to moderate contusion injury induced approximately 3,000 myelinated fibers to extend into the lesion at 12 weeks (46). In addition, the number of axons in the channels far exceeded the number of axons that regenerated after implantation of PN grafts in the Cheng et al. (13) study including those in our laboratory (25, 50). There are several recent reports of the grafting of PNs into the spinal cord in a small number of humans with subacute or chronic SCI. This strategy has been found to be feasible, although no randomized, controlled trials have been performed in humans (14, 45, 53).

Origin of the Regenerated or Sprouted Axons

Although the precise origin and destination of the regenerated axons in the channels are unknown, our axonal tracing and morphometric findings suggest that many of the regenerated axons in the channels originated locally, such as from neurons in the DRGs adjacent to the tissue bridges. First, there were many CGRP-immunolabeled axons in the bridges, and it is known that 66% of the DRG neurons in rodents are immunopositive for CGRP (20). Also, 40.7% of the fibers in the PN grafts were 2 to 5 μm in diameter, and most of the regenerated fibers in Groups SA+C+PN, SA+EC, and CH+C+PN were in this range (Fig. 9D). It is known that central nervous system fibers are much smaller than peripheral nervous system fibers. For example, the fiber diameter in the rat sciatic nerve is approximately 7 μm , comparable to the PN grafts in the present study (51), whereas the fiber diameter in the dorsal, lateral, and ventral columns and the corticospinal tract in the rat spinal

cord are approximately 2.4, 3.1, 4.1, and 1.1 μm , respectively (8, 28). However, we found that the PN grafts also contained many small fibers less than 5 μm , corresponding to the size of the majority of the regenerated fibers in the bridges. In addition, anterograde labeling with BDA revealed no evidence that the axons in the channels originated from the corticospinal tract. Other investigators also found that the majority of regenerated axons in PN grafts implanted after SCT or hemisection originated from neurons in the DRGs adjacent to the tissue bridges or from local neurons in the adjacent spinal cord (38–40). However, we cannot rule out the possibility that some of the regenerated fibers in the present study originated from anterior horn cells or segmental sensory neurons in the spinal cord, which may have resulted in local motor or sensory improvements that would not have been detected by the functional tests that we employed. Moreover, our techniques could not distinguish between axons in the channel that sprouted from adjacent spared axons and those that regenerated from transected axons. Future studies should include additional axonal tracing with anterograde tracers from a larger number of sites, including the brainstem and retrograde tracing from the spinal cord and DRGs.

Schwann Cell Survival

PN grafts from GFP rats facilitated identification of grafted versus host Schwann cells. All axons in the tissue bridges 14 weeks after PN grafting are host axons from the central nervous system or nerve roots because donor axons in the PN grafts do not survive as indicated above, and it is known that NF200 immunoreactivity in the distal portion of the completely severed PN disappears within 2 weeks after axotomy (29). Fourteen weeks after the implantation of PN-filled channels, we observed numerous p75-positive, GFP-expressing Schwann cells within the bridges that were closely associated with regenerating host axons. Interestingly, there were only a small number of astrocytes and no oligodendrocytes in the bridges. Schwann cells can survive in the presence of degenerating axons for 1 year (58), and it has been widely accepted that Schwann cells are capable of facilitating central axonal regrowth after SCI (33). Schwann cells can act as a cellular scaffold in the lesion, but they also produce various neurotrophic factors, synthesize extracellular matrix, and express a variety of cell adhesion molecules to promote repair of the damaged spinal cord (52). PN grafting (13, 25, 39) or transplantation of cultured Schwann cells in tubular guidance channels has been a frequent strategy for spinal repair, either alone or in combination with neuroprotective agents (12), neurotrophic factors (3, 27), chondroitinase ABC (11, 15), or grafts of olfactory ensheathing glia (35), but functional recovery has been minimal. Schwann cell transplantation has also been attempted for chronic SCI (19, 37), but recovery was not determined. Recently, it was shown that approximately 17% of transplanted cultured Schwann cells survived for 3 months after transplantation in the cavity in a chronic SCI model (4). We can estimate the number of surviving Schwann cells based on the 1:1 association of Schwann cells with myelinated fibers and the pattern in PNs. In the PN control, there were approximately 50,000 myelinated axons (Table

2), and in the subacute and chronic groups (Groups SA+C+PN and CH+C+PN), there were approximately 35,000 and 26,000 axons, respectively. Thus, we estimate that 50 to 70% of the Schwann cells survived, assuming no proliferation of Schwann cells during this time. This was confirmed by the finding of no Ki67-labeled Schwann cells in the channels at 14 weeks, although there was likely some proliferation earlier (30). Also, survival rates of 50 to 70% of Schwann cells do not include Schwann cells associated with nonmyelinated fibers or any host Schwann cells that may have migrated from adjacent spinal roots or DRG. There were only a small number of host Schwann cells in the tissue bridges in rats in Group SA+EC, and therefore we do not expect that a large number of host Schwann cells migrated into the tissue bridges in Groups SA+C+PN and CH+C+PN. According to the G ratios of Groups SA+C+PN and CH+C+PN (23), most of the axons in the bridges had well developed myelin, indicating excellent functional capacity of the surviving Schwann cells.

Migration of Donor Schwann Cells

Donor Schwann cells do not migrate into the adjacent host spinal cord after transplantation (4). In the present study, we also observed no migration of donor Schwann cells from the PN grafts into the rostral or caudal spinal cord adjacent to the bridges. However, some donor Schwann cells migrated out of the channels and along the external surface of the channel wall, and these cells were associated with some axons indicating that donor Schwann cells are capable of migrating when an adequate scaffold is present.

Inflammation and Biocompatibility of the Chitosan Channels

There were no inflammatory cells in the channel walls and minimal inflammatory or fibrotic reaction adjacent to the channel walls, indicating good biocompatibility of the chitosan channels. In contrast, in our previous study of implanted synthetic poly(2-hydroxyethyl methacrylate-comethylmethacrylate) and poly(2-hydroxyethyl methacrylate) PN-filled channels in a SCT model, we found atrophy of the grafted PNs and sparse axonal regrowth (30). In the present study, the chitosan channels (92% deacetylated) remained intact in the cavity for 14 weeks. This is consistent with another study that demonstrated biostability of 93.3% deacetylated implanted chitosan in the skin for 12 weeks (4). Slow degradation coupled with excellent biocompatibility of the chitosan likely contributed to the long survival of the donor Schwann cells in the present experiment. These properties make chitosan one of the most promising biomaterials for SCI repair.

Functional Recovery

Despite the large number of regenerated axons in the bridges, there was no functional recovery on the basis of open-field locomotor testing. Similarly, Le Beau et al. (24) found no motor recovery with silicone tubes and PN transplants and suggested that constrictive forces based on the collapse of tubes caused axonal degeneration. In contrast, the chitosan channels in the present study remained concentric, did not collapse, and

contained regenerating axons that were morphologically intact. Future study of this strategy should also include examination of local motor recovery to detect regeneration of local motor neurons as well as sensory recovery. Such recovery would have major functional significance if it enhanced local motor or sensory recovery in injuries involving cervical or lumbar spinal cord. Sensory tests could also assess the presence of allodynia. It would also be of interest to examine functional recovery after injuries of less severity. To attract more supraspinal axons, combined therapy with other agents will likely be necessary, such as the application of antibodies against Nogo-A (5) and administration of cyclic adenosine monophosphate (2, 27), chondroitinase ABC, or neurotrophic factors.

Potential Limitations

Two injured control groups were employed for evaluating the chitosan plus PN strategy: an empty channel group and a group without channels. We reasoned that an additional control group of PN grafts without channels was not necessary to address the first hypothesis that axonal regeneration in a chitosan tube is enhanced by adding PN grafts to the tube. Similarly, this additional control was not necessary to address the second hypothesis that chitosan channels have good biocompatibility in the injured spinal cord. Previous studies of peripheral nerve grafts alone in our laboratory (50) and other laboratories (39, 40, 47), and grafting of Schwann cells alone produced only minimal functional recovery and modest axonal regrowth from brainstem motor nuclei (10, 26, 56). Also, a recent study in an SCI model similar to ours showed that, although intracavitary transplantation of autologous PN grafts 1 week after SCI promoted axonal regeneration past the lesion site, there was no functional recovery (37).

REFERENCES

- Archelos JJ, Roggenbuck K, Schneider-Schaulies J, Toyka KV, Hartung HP: Detection and quantification of antibodies to the extracellular domain of P0 during experimental allergic neuritis. *J Neurol Sci* 117:197-205, 1993.
- Bakshi A, Hunter C, Swanger S, Lepore A, Fischer I: Minimally invasive delivery of stem cells for spinal cord injury: Advantages of the lumbar puncture technique. *J Neurosurg Spine* 1:330-337, 2004.
- Bamber NL, Li H, Lu X, Oudega M, Aebischer P, Xu XM: Neurotrophins BDNF and NT-3 promote axonal re-entry into the distal host spinal cord through Schwann cell-seeded mini-channels. *Eur J Neurosci* 13:257-268, 2001.
- Barakat DJ, Gaglani SM, Neravetla SR, Sanchez AR, Andrade CM, Pressman Y, Puzis R, Garg MS, Bunge MB, Pearse DD: Survival, integration, and axon growth support of glia transplanted into the chronically contused spinal cord. *Cell Transplant* 14:225-240, 2005.
- Bareyre FM, Kerschensteiner M, Raineteau O, Mettenleiter TC, Weinmann O, Schwab ME: The injured spinal cord spontaneously forms a new intraspinal circuit in adult rats. *Nat Neurosci* 7:269-277, 2004.
- Basso DM, Beattie MS, Bresnahan JC: A sensitive and reliable locomotor rating scale for open field testing in rats. *J Neurotrauma* 12:1-21, 1995.
- Bradbury EJ, Moon LD, Popat RJ, King VR, Bennett GS, Patel PN, Fawcett JW, McMahon SB: Chondroitinase ABC promotes functional recovery after spinal cord injury. *Nature* 416:636-640, 2002.
- Brösamle C, Schwab ME: Ipsilateral, ventral corticospinal tract of the adult rat: Ultrastructure, myelination and synaptic connections. *J Neurocytol* 29:499-507, 2000.
- Bunge MB: Bridging areas of injury in the spinal cord. *Neuroscientist* 7:325-339, 2001.
- Bunge MB: Bridging the transected or contused adult rat spinal cord with Schwann cell and olfactory ensheathing glia transplants. *Prog Brain Res* 137:275-282, 2002.
- Chau CH, Shum DK, Li H, Pei J, Lui YY, Wirthlin L, Chan YS, Xu XM: Chondroitinase ABC enhances axonal regrowth through Schwann cell-seeded guidance channels after spinal cord injury. *FASEB J* 18:194-196, 2004.
- Chen A, Xu XM, Kleitman N, Bunge MB: Methylprednisolone administration improves axonal regeneration into Schwann cell grafts in transected adult rat thoracic spinal cord. *Exp Neurol* 138:261-276, 1996.
- Cheng H, Cao Y, Olson L: Spinal cord repair in adult paraplegic rats: Partial restoration of hind limb function. *Science* 273:510-513, 1996.
- Cheng H, Liao KK, Liao SF, Chuang TY, Shih YH: Spinal cord repair with acidic fibroblast growth factor as a treatment for a patient with chronic paraplegia. *Spine* 29:E284-E288, 2004.
- Fouad K, Schnell L, Bunge MB, Schwab ME, Liebscher T, Pearse DD: Combining Schwann cell bridges and olfactory-ensheathing glia grafts with chondroitinase promotes locomotor recovery after complete transection of the spinal cord. *J Neurosci* 25:1169-1178, 2005.
- Freier T, Jimenez-Hamann M, Katayama Y, Musoke-Zawedde P, Piotrowicz A, Yuan Y, Shoichet MS, Midha R: *Biodegradable Polymers in Neural Tissue Engineering*. Ames, American Scientific Publishers, 2005, pp 141-189.
- Friedman JA, Windebank AJ, Moore MJ, Spinner RJ, Currier BL, Yaszemski MJ: Biodegradable polymer grafts for surgical repair of the injured spinal cord. *Neurosurgery* 51:742-755, 2002.
- Gautier SE, Oudega M, Frago M, Chapon P, Plant GW, Bunge MB, Parel JM: Poly(alpha-hydroxyacids) for application in the spinal cord: Resorbability and biocompatibility with adult rat Schwann cells and spinal cord. *J Biomed Mater Res* 42:642-654, 1998.
- Hill CE, Moon LD, Wood PM, Bunge MB: Labeled Schwann cell transplantation: Cell loss, host Schwann cell replacement, and strategies to enhance survival. *Glia* 53:338-343, 2006.
- Hiruma H, Saito A, Ichikawa T, Kiriya Y, Hoka S, Kusakabe T, Kobayashi H, Kawakami T: Effects of substance P and calcitonin gene-related peptide on axonal transport in isolated and cultured adult mouse dorsal root ganglion neurons. *Brain Res* 883:184-191, 2000.
- Iannotti C, Li H, Yan P, Lu X, Wirthlin L, Xu XM: Glial cell line-derived neurotrophic factor-enriched bridging transplants promote propriospinal axonal regeneration and enhance myelination after spinal cord injury. *Exp Neurol* 183:379-393, 2003.
- Itoh S, Matsuda A, Kobayashi H, Ichinose S, Shinomiya K, Tanaka J: Effects of a laminin peptide (YIGSR) immobilized on crab-tendon chitosan tubes on nerve regeneration. *J Biomed Mater Res B Appl Biomater* 73:375-382, 2005.
- Katayama Y, Montenegro R, Freier T, Midha R, Belkas JS, Shoichet MS: Coil-reinforced hydrogel tubes promote nerve regeneration equivalent to that of nerve autografts. *Biomaterials* 27:505-518, 2006.
- Le Beau JM, Ellisman MH, Powell HC: Ultrastructural and morphometric analysis of long-term peripheral nerve regeneration through silicone tubes. *J Neurocytol* 17:161-172, 1988.
- Lee YS, Lin CY, Robertson RT, Hsiao I, Lin VW: Motor recovery and anatomical evidence of axonal regrowth in spinal cord-repaired adult rats. *J Neuropathol Exp Neurol* 63:233-245, 2004.
- Martin D, Robe P, Franzen R, Delrée P, Schoenen J, Stevenaert A, Moonen G: Effects of Schwann cell transplantation in a contusion model of rat spinal cord injury. *J Neurosci Res* 45:588-597, 1996.
- Meijs MF, Timmers L, Pearse DD, Tresco PA, Bates ML, Joosten EA, Bunge MB, Oudega M: Basic fibroblast growth factor promotes neuronal survival but not behavioral recovery in the transected and Schwann cell implanted rat thoracic spinal cord. *J Neurotrauma* 21:1415-1430, 2004.
- Nashmi R, Fehlings MG: Changes in axonal physiology and morphology after chronic compressive injury of the rat thoracic spinal cord. *Neuroscience* 104:235-251, 2001.
- Nomura H, Furuta A, Iwaki T: Dorsal root rupture injury induces extension of astrocytic processes into the peripheral nervous system and expression of GDNF in astrocytes. *Brain Res* 950:21-30, 2002.
- Nomura H, Katayama Y, Shoichet MS, Tator CH: Complete spinal cord transection treated by implantation of a reinforced synthetic hydrogel channel results in syringomyelia and caudal migration of the rostral stump. *Neurosurgery* 59:183-192, 2006.

31. Nomura H, Tator CH, Shoichet MS: Bioengineered strategies for spinal cord repair. *J Neurotrauma* 23:496–507, 2006.
32. Oudega M, Gautier SE, Chapon P, Fragoso M, Bates ML, Parel JM, Bunge MB: Axonal regeneration into Schwann cell grafts within resorbable poly(alpha-hydroxyacid) guidance channels in the adult rat spinal cord. *Biomaterials* 22:1125–1136, 2001.
33. Oudega M, Xu XM: Schwann cell transplantation for repair of the adult spinal cord. *J Neurotrauma* 23:453–467, 2006.
34. Pinzon A, Calancie B, Oudega M, Noga BR: Conduction of impulses by axons regenerated in a Schwann cell graft in the transected adult rat thoracic spinal cord. *J Neurosci Res* 64:533–541, 2001.
35. Ramón-Cueto A, Cordero MI, Santos-Benito FF, Avila J: Functional recovery of paraplegic rats and motor axon regeneration in their spinal cords by olfactory ensheathing glia. *Neuron* 25:425–435, 2000.
36. Ramón-Cueto A, Plant GW, Avila J, Bunge MB: Long-distance axonal regeneration in the transected adult rat spinal cord is promoted by olfactory ensheathing glia transplants. *J Neurosci* 18:3803–3815, 1998.
37. Rasouli A, Bhatia N, Suryadevara S, Cahill K, Gupta R: Transplantation of preconditioned Schwann cells in peripheral nerve grafts after contusion in the adult spinal cord. Improvement of recovery in a rat model. *J Bone Joint Surg Am* 88A:2400–2410, 2006.
38. Richardson PM, Issa VM, Aguayo AJ: Regeneration of long spinal axons in the rat. *J Neurocytol* 13:165–182, 1984.
39. Richardson PM, McGuinness UM, Aguayo AJ: Axons from CNS neurons regenerate into PNS grafts. *Nature* 284:264–265, 1980.
40. Richardson PM, McGuinness UM, Aguayo AJ: Peripheral nerve autografts to the rat spinal cord: Studies with axonal tracing methods. *Brain Res* 237:147–162, 1982.
41. Ridet JL, Malhotra SK, Privat A, Gage FH: Reactive astrocytes: Cellular and molecular cues to biological function. *Trends Neurosci* 20:570–577, 1997.
42. Rivlin AS, Tator CH: Effect of duration of acute spinal cord compression in a new acute cord injury model in the rat. *Surg Neurol* 10:38–43, 1978.
43. Rosales-Cortés M, Peregrina-Sandoval J, Bañuelos-Pineda J, Castellanos-Martínez EE, Gómez-Pinedo UA, Albarrán-Rodríguez E: Regeneration of the axotomized sciatic nerve in dogs using the tubulisation technique with chitosan biomaterial preloaded with progesterone [in Spanish]. *Rev Neurol* 36:1137–1141, 2003.
44. Silver J, Miller JH: Regeneration beyond the glial scar. *Nat Rev Neurosci* 5:146–156, 2004.
45. Tadie M, Liu S, Robert R, Guiheneuc P, Pereon Y, Perrouin-Verbe B, Mathe JF: Partial return of motor function in paralyzed legs after surgical bypass of the lesion site by nerve autografts three years after spinal cord injury. *J Neurotrauma* 19:909–916, 2002.
46. Takami T, Oudega M, Bates ML, Wood PM, Kleitman N, Bunge MB: Schwann cell but not olfactory ensheathing glia transplants improve hindlimb locomotor performance in the moderately contused adult rat thoracic spinal cord. *J Neurosci* 22:6670–6681, 2002.
47. Tator CH: Review of treatment trials in human spinal cord injury: Issues, difficulties, and recommendations. *Neurosurgery* 59:957–987, 2006.
48. Tsai EC, Dalton PD, Shoichet MS, Tator CH: Matrix inclusion within synthetic hydrogel guidance channels improves specific supraspinal and local axonal regeneration after complete spinal cord transection. *Biomaterials* 27:519–533, 2006.
49. Tsai EC, Dalton PD, Shoichet MS, Tator CH: Synthetic hydrogel guidance channels facilitate regeneration of adult rat brainstem motor axons after complete spinal cord transection. *J Neurotrauma* 21:789–804, 2004.
50. Tsai EC, Krassioukov AV, Tator CH: Corticospinal regeneration into lumbar grey matter correlates with locomotor recovery after complete spinal cord transection and repair with peripheral nerve grafts, fibroblast growth factor 1, fibrin glue, and spinal fusion. *J Neuropathol Exp Neurol* 64:230–244, 2005.
51. Varejão AS, Cabrita AM, Meek MF, Bulas-Cruz J, Melo-Pinto P, Raimondo S, Geuna S, Giacobini-Robecchi MG: Functional and morphological assessment of a standardized rat sciatic nerve crush injury with a non-serrated clamp. *J Neurotrauma* 21:1652–1670, 2004.
52. Venstrom KA, Reichardt LF: Extracellular matrix. 2: Role of extracellular matrix molecules and their receptors in the nervous system. *FASEB J* 7:996–1003, 1993.
53. von Wild KR, Brunelli GA: Restoration of locomotion in paraplegics with aid of autologous bypass grafts for direct neurotisation of muscles by upper motor neurons—The future: Surgery of the spinal cord? *Acta Neurochir Suppl* 87:107–112, 2003.
54. Weidner N, Ner A, Salimi N, Tuszynski MH: Spontaneous corticospinal axonal plasticity and functional recovery after adult central nervous system injury. *Proc Natl Acad Sci U S A* 98:3513–3518, 2001.
55. Woerly S, Doan VD, Evans-Martin F, Paramore CG, Peduzzi JD: Spinal cord reconstruction using NeuroGel implants and functional recovery after chronic injury. *J Neurosci Res* 66:1187–1197, 2001.
56. Xu XM, Zhang SX, Li H, Aebischer P, Bunge MB: Regrowth of axons into the distal spinal cord through a Schwann-cell-seeded mini-channel implanted into hemisectioned adult rat spinal cord. *Eur J Neurosci* 11:1723–1740, 1999.
57. Yoshii S, Oka M, Shima M, Taniguchi A, Taki Y, Akagi M: Restoration of function after spinal cord transection using a collagen bridge. *J Biomed Mater Res* 70:569–575, 2004.
58. You S, Petrov T, Chung PH, Gordon T: The expression of the low affinity nerve growth factor receptor in long-term denervated Schwann cells. *Glia* 20:87–100, 1997.
59. Yuan Y, Zhang P, Yang Y, Wang X, Gu X: The interaction of Schwann cells with chitosan membranes and fibers in vitro. *Biomaterials* 25:4273–4278, 2004.

Acknowledgments

This work was supported by a Grant-in-Aid from the Ontario Neurotrauma Foundation (Fellowship grant 2004-SCI-FS-28 awarded to HN), by the Natural Sciences and Engineering Research Council of Canada (to MSS, CM, CHT), and by operating funds from the Canadian Paraplegic Association (Ontario Branch). We thank Rita van Bendegem, Linda Lee, Thomas Freier, Ph.D., Howard Kim, Tony Collins, Ph.D., Peter Poon, Michael Jonathan Wan, and James Correia for their excellent technical assistance; Armand Keating, M.D., F.R.C.P.C., for providing the GFP rats; and Sheer Ramjohn for outstanding expertise in electron microscopy.

COMMENTS

This article evaluates the efficacy of an intramedullary implant in promoting axon regeneration in a rat model of crush injury to the thoracic spinal cord. The intramedullary implant used is a synthetic tube of chitosan (a biodegradable polysaccharide) filled with donor peripheral nerve grafts from green fluorescent protein (GFP)-labeled animals. The chitosan channels with peripheral nerve grafts, as well as appropriate controls, were implanted into the traumatic cord cavitation in a delayed fashion 1 or 4 weeks after injury. The animals were evaluated for functional recovery over a period of 12 weeks by blinded observers and subsequently were sacrificed for histological examination.

The implants had no impact on functional recovery, as no animals were able to bear weight on their hindlimbs. On histological examination, a tissue bridge with several thousand axons was noted in the implanted chitosan channels with peripheral nerve grafts, most prominently in the animals that received the implants 1 week after injury.

The regenerated axons in the tissue bridge do not seem to come from the corticospinal tract, as Nomura et al. demonstrated with anterograde BDA labeling. They hypothesized that the axons stem from cell bodies in the dorsal root ganglion or rostral cord. With GFP labeling of the peripheral nerve grafts, they showed that donor Schwann cells are intimately related with the process of axonal regeneration.

This study adds to a growing body of literature on biosynthetic implants designed to heal spinal cord injury. It is encouraging that a robust number of axons are seen within the implants at the 12-week follow-up, but disappointing that no regeneration of the corticospinal tracts was seen and that no functional recovery occurred.

Vikram Nayar
Daniel H. Kim
Houston, Texas

This article describes the implantation of chitosan channels containing peripheral nerve grafts into trauma-created gaps in the spinal cord. Although no functional benefit was noted, Nomura et al. were able to detect robust axonal growth through the graft. Using GFP-labeled donor animals, they were able to demonstrate remyelination of these axons within the graft; however, there was no evidence of spreading of the GFP Schwann cells beyond the border of the chitosan graft. Overall, this work is important in that it describes a technique for using genetically altered animals as donors to trace the fate of transplanted cells. The robust axonal growth is encouraging; however, the lack of any functional improvement and the fact that cavities rostral and caudal to the cord persisted limits the celebration at this point. I would be curious to see a more detailed description of where the axons were coming from and where they were going. Otherwise, this is well-done work.

Daniel K. Resnick
Madison, Wisconsin

Findings of this laboratory investigation include the following: 1) implanted chitosan channels have no significant degradation or immune/tissue reaction at 3 months when implanted into the spinal cord, 2) robust axonal infiltration with myelination by Schwann cells occurs in these channels when they are filled with peripheral nerve grafts (seen both at 1 and 4 weeks after crush injury), 3) Schwann cells do not migrate into the adjacent spinal cord, 4) there is no evidence of corticospinal tract regeneration into or across the channels filled with nerve grafts, and 5) no functional benefit in the experimental groups was observed with serial locomotor testing. These are all important contributions to the optimization and/or development of peripheral nerve conduits for the treatment of spinal cord injury.

Although not directly confirmed, the extensive infiltration of axons in the channels were presumably from local spinal cord neurons or, more likely, from nearby dorsal root ganglia. Future investigations should include tracer studies examining the origin and destination of these axons, as well as functional assessment of pain and sensation, the latter of which was mentioned by Nomura et al. It is unfortunate, albeit not surprising, that there was no evidence of corticospinal tract regeneration across the injury site, either histologically or functionally. They mention the addition of various factors to help overcome this problem, including, for example, antibodies to Nogo-A or chondroitinases. The effect of these factors on promotion of corticospinal tract regeneration, however, remains somewhat complicated and disappointing. Furthermore, the reasons that corticospinal tract axons do not regenerate into a peripheral nerve graft may be distinct from those preventing regeneration in the central nervous system itself. Some authors have been experimenting with peripheral nerve grafts from the spinal cord directly to peripheral nerves. Although the results of Nomura et al. provide evidence that this repair concept may be flawed because corticospinal tract neurons did not enter the peripheral nerve grafts at all in this study, we know that what is at the end of the channel or graft is also very important. Perhaps having a peripheral nerve or an eventual motor endplate at the distal end of the channel may promote motor regeneration, as opposed to the spinal cord being at the other end. Nevertheless, the abrupt lack of any corticospinal tract axons entering the peripheral nerve grafts in the current study is of concern.

Nomura et al. comment that the chitosan channels may be advantageous because they do not degrade or collapse by approximately 3 months. With such robust axonal infiltration and myelination present by 3 months, is it possible that the channels may, in fact, not degrade quickly enough? In viewing *Figure 2* of the article, there is a halo of what appears to be dead space between the clumped grafts and the channel (presumably not artifact); perhaps some collapse would be

acceptable. However, this may be a moot point considering there was no significant immune or tissue reaction to the chitosan channels at the time points examined.

Nomura et al. have presented a sound and meticulous preliminary investigation of their experimental model.

Stephen M. Russell
New York, New York

Nomura et al. examined a strategy to promote axonal regeneration after subacute spinal cord injury consisting of intramedullary implantation of chitosan guidance channels containing peripheral nerve grafts. Fourteen weeks after implantation, these channels were found to contain a thick bridge of myelinated axons in both the subacute and chronic groups. The axons appeared to be from the dorsal root ganglion. Additionally, approximately half of the Schwann cells that accompanied the nerve grafts survived at the end of the experiment. No inflammatory response to the chitosan was noted. Although this treatment did not seem to improve the functional outcome of the animals, the findings are quite encouraging and exciting. The authors plan a series of future experiments that will certainly shed more light on this technique.

Vincent C. Traynelis
Iowa City, Iowa

Dr. Tator and his group continue to present meticulous studies as they attack some of the most complex and challenging problems in spinal cord injury. Even the unfamiliar reader will be able to tell with a glance the amount of detail that has gone into every possible aspect of this experiment. To successfully apply such a multitude of objective outcome measures in such a delicate model of spinal cord injury is truly a hallmark of the work Dr. Tator and his team are known for. Those of us with experience in this field can only be amazed.

The results of this study are as exciting as they are inspiring. Although the objectives of the research questions have clearly been accomplished in that chitosan guidance tubules are reliable and function best when loaded with peripheral nerve grafts, the perhaps unexpected number of regenerating axons and Schwann cells induced in this contusion model is certainly a cause for a degree of optimism. Even though functional benefit has not yet been accomplished and other limitations exist (as appropriately explored in the article) another door in the maze of spinal cord injury has been unlocked and opened, a door that will serve as a corridor for much more research to come, no doubt by this group and by many others as well.

R. John Hurlbert
Calgary, Canada

Nomura et al. have illustrated nicely that a biodegradable polymeric scaffold may be useful to structurally guide axonal regeneration in a rodent model. They used chitosan, a polysaccharide derivative of chitin from crustacean exoskeletons, which has recently been applied in bioengineering. Chitosans have been used experimentally to create nanostructures for nonviral gene transfection, skin substitutes, hemostatic agents, and drug delivery systems. They benefit from being easy to shape and mass produce and have also been found to be highly biocompatible.

More recently, the use of chitosan to produce a mechanical conduit for peripheral nerve regrowth has been explained, and Nomura et al. have described in this report an extension of this concept to spinal cord injury. Their experimental model used intercostal nerve autografts that were applied within the polysaccharide scaffold into a previous area of clip-induced spinal cord injury. The histological results were

impressive, with the demonstration of axonal regrowth through the manufactured conduit on electron microscopy. There was no associated functional recovery, which was not altogether surprising, given their model of spinal cord injury.

Ultimately, combinatorial strategies will probably be necessary to bring us to the next step to realize reliable functional improvements in

animal models. Nomura et al. have presented their well-conceived and conducted work, and I look forward to further advances from their laboratory in polymer bioproducts to enhance neural recovery.

Michael Y. Wang
Miami, Florida



Pioneers of Cancer Treatment: Surgery. Christian Albert Theodor Billroth (1829–1894) was a pioneer in the treatment of cancer of internal organs. Having been made Professor of Surgery at Zurich and then at Vienna, he spent his life achieving many surgical triumphs, including resection of the esophagus, complete excision of the larynx, partial gastrectomy, and gastrojejunostomy. Each year, Billroth published his surgical results. Alexandre von Winiwarter, his assistant, compiled these data and published them as one of the first statistical reviews of operative results in cancer. From Shimkin MB: *Contrary to Nature: Being an Illustrated Commentary on Some Persons and Events of Historical Importance in the Development of Knowledge Concerning Cancer*. Washington D.C., U.S. Department of Health, Education, and Welfare, 1977.